Temperature Gradients in the Channels of a Single-Screw Extruder

ANTHONY J. BUR* *and* STEVEN C. ROTH

National Institute of Standards and Technology
Gaithersburg, MD 20899-8542

MARK A. SPALDING, DANIEL W. BAUGH, KURT A. KOPPI,
and WALTER C. BUZANOWSKI

The Dow Chemical Company
Midland, MI 48674

We used a temperature-sensitive fluorescent dye, perylene, to monitor the true resin temperature during extrusion of polycarbonate. The measurement involved doping polycarbonate with perylene and detecting fluorescence with an optical sensor that accesses a standard instrumentation port on a barrel of a single-screw extruder. The sensor's confocal optics design permits fluorescence intensity measurements as a function of position. Using a previously established calibration function, temperature and temperature gradients were obtained from the measured fluorescence. Because the origin of the measurement is the fluorescent dye molecule that is soluble in the resin, this method allows temperature measurement of the polymer without interference from the surrounding metal parts. With the sensor looking over the screw, temperature profiles from the barrel wall to the core of the screw were obtained as a function of screw speed, screw design and resin melt flow rate. Polym. Eng. Sci. 44:2148–2157, 2004.

INTRODUCTION

The temperature of a molten polymer stream is a key processing parameter to know for all processes. The process temperature affects many critical material parameters including the viscosity, density of the resin, and degradation kinetics (1). The temperature of the molten resin, however, is rarely known with great accuracy because of problems associated with thermocouples, the most common instrument for temperature measurement. In commercial processes, thermocouples transfer energy readily to and from the equipment and thus are highly influenced by the temperature of the surrounding metal.

Numerous methods have been developed to minimize the energy transfer associated with thermocouple use (2–7). The most common method is to place small thermocouples in a bridge assembly that intersects the flow in a transfer pipe. For this arrangement, the thermocouples are imbedded into a high-temperature polymeric support bridge and the thin thermocouple wires are aligned in the flow direction for a short distance, (6–8) or a matrix of thermocouple junctions are formed from intersecting wires that have been welded together and supported in the flow stream (2, 3). These bridges provide an accurate temperature measurement of the flow, but the devices are extremely delicate and cannot be used to measure temperatures inside an extruder. Esseghir and Sernas (9) developed a mechanical system to insert and retract a small thermocouple through a barrel wall of a lab extruder to measure the temperature in a rotating screw channel. For this system, the thermocouple was inserted and then retracted for each rotation to allow the screw flight to pass. As with the thermocouple bridge, this system is very delicate and only for lab use. Moreover, conduction of energy from the surrounding metal will influence the measurement in the channel. This research was performed using a model fluid (corn syrup), at nearly ambient conditions, and the probe was invasive to the flow path.

*To whom correspondence should be addressed. E-mail: abur@nist.gov
†This paper is a contribution from the National Institute of Standards and Technology, and, thus, is not subject to copyright in the United States.

Published online in Wiley InterScience (www.interscience.wiley.com).
DOI: 10.1002/pen.20221

Several non-invasive methods exist for temperature measurement including infrared (IR) (10, 11) and fluorescence techniques (12–14). Infrared measurements are not capable of measuring the temperature as a function of distance away from the sensor. Fluorescent dyes offer a unique and non-invasive method of temperature measurement. In practice, the dye is mixed with resin at dopant concentrations, less than 10^{-4} mass concentration of dye in the resin. Because the dye is soluble in the resin at processing temperatures it acts as a molecular probe, responding to the resin molecular environment in which it exists, and the observed spectra indicate local environmental conditions. Thus, a temperature deduced from fluorescence spectra is the true resin temperature. The fluorescence method used here employs a sensor with confocal optics, permitting temperature measurements at different distances from the sensor tip; i.e., a temperature profile (14).

The goal of this work is to apply fluorescence temperature measuring techniques to single-screw extrusion. Temperature measurements made deep into rotating metering channels as a function of screw speed, screw design, and melt flow rate (MFR) for polycarbonate (PC) resins are presented.

EXPERIMENTAL PROCEDURES (15)

Materials

Two commercial-grade PC resins manufactured by The Dow Chemical Company were used for this study. They had melt flow rates (MFR) of 6 g/10 min and 23 g/10 min (ASTM D-1238, Condition O, 300°C, 1.2 kg). These resins were used previously in a melting rate study (16). The fluorescent dye, perylene, was obtained from Aldrich and was used as received. The resins were dried, compounded using a twin-screw extruder with 1.6×10^{-5} mass fraction of perylene dye, and then repelletized. The perylene-PC compounded resin pellets were dried overnight at 122°C in dehumidifying desiccant dryers prior to extrusion. Shear viscosities of the resins at 280°C are shown in *Fig. 1*.

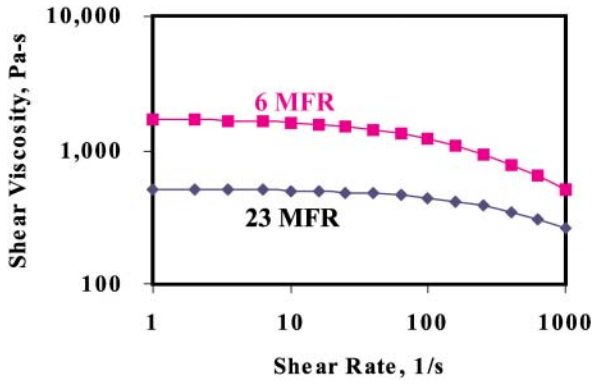

Fig. 1. The viscosity versus shear rate for the MFR 6 and MFR 23 polycarbonate resins at 280°C. [Color figure can be viewed in the online issue, which is available at www.interscience.wiley.com.]

Measuring Equipment

A highly instrumented, 63.5-mm-diameter single-screw extruder with a 21 length-to-diameter ratio (L/D) was used to collect extrusion process data. This extruder had eleven pressure transducers along the axis of the barrel to measure pressures along the screw. The pressure sensor positioned at 19 diameters (position P19) from the start of the screw was removed and replaced with a fluorescence optical sensor. The extruder was equipped with three barrel temperature control zones. The barrel temperatures were set at 275°C for all zones.

A conventional single-flighted and square-pitched screw with a compression ratio of 2.8 was used for most of the studies (17). The screw had a feed depth of 8.9 mm for 6 diameters, a transition length of 8 diameters, and a meter depth of 3.18 mm for 7 diameters. The specific drag flow rate, that is the specific rate expected for just rotation with no imposed pressure gradients, was calculated at 8.98 kg/(h·rad/s) or 0.94 kg/(h·rpm), where rpm is revolutions per minute. The optical temperature sensor was positioned over the constant depth metering section. Previous work indicated that these PC resins were completely molten at this barrel position for this screw at screw speeds of 60 rpm and less (16).

A high-performance Energy Transfer screw was also used for this study (18–20). This screw is referred to as the mixing screw in the remainder of the paper. A previous description of this screw (20) is reiterated here for clarity. The mixing screw had a lead length of 76.2 mm and a primary flight clearance of 0.08 mm. It had an 8-diameter-long feed section that was 10.9 mm deep, a 6-diameter transition section, and a 7-diameter-long mixing section. The feed and transition sections were single-flighted, and the mixing section, shown in *Fig. 2*, was designed with two channels. The channel depths were 3.18 mm at the entrance and exit of the mixing section, and within the mixing section they oscillated between 1.45 mm and 6.35 mm. The period of these oscillations was out of phase for the two channels. In addition, the flights between the channels were undercut to 1.40 mm deep at strategic locations so that flow could occur between the channels. The specific drag rate was calculated at 9.26 kg/(h·rad/s) or 0.97 kg/(h·rpm). The optical sensor was positioned over the top of the mixing section and it was observing both channels. The depth of the channels as viewed by the optical sensor is shown by *Fig. 3*.

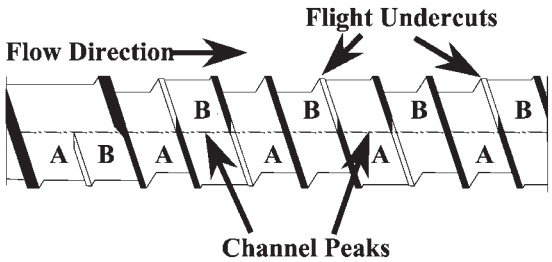

Fig. 2. A drawing of the mixing screw.

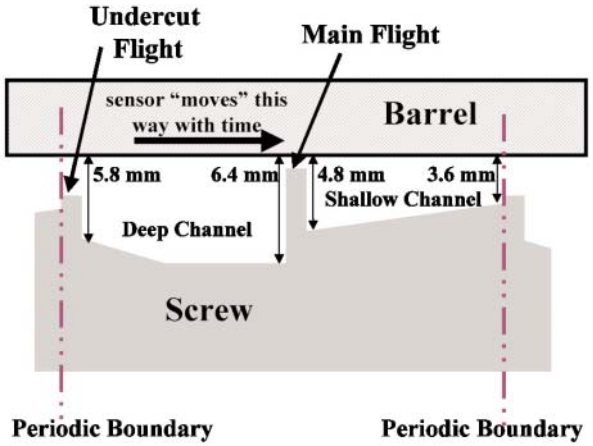

Fig. 3. Channel depths for the 63.5-mm-diameter mixing screw as viewed by the fluorescence optical sensor. [Color figure can be viewed in the online issue, which is available at www.interscience.wiley.com.]

Both the conventional and mixing screws were built with 60° angled tips at the discharge ends. These tips were matched to a conical transfer line adapter. The transfer line adapter had an angle of 60°, such that the clearance between the start of the tip and the conical adapter wall was constant and fixed at 6 mm. The transfer line was 9.5 mm in diameter.

A smaller 19-mm-diameter single-screw extruder was used in validation experiments to establish measuring credentials for the fluorescence temperature technique. The extruder had an L/D = 22 and was equipped with a conventional feeding and metering screw with a channel depth at the metering end of 2 mm. For the validation experiments, this extruder was instrumented with pressure, thermocouple and fluorescence sensors and a Dynisco IR (infrared) radiometer.

The light source for the fluorescence sensor was a 30-mW, 407-nm diode laser from Power Technologies. Laser light was filtered with a 10-nm bandpass filter centered at 405 nm and focused onto a single 200-μm-diameter optical fiber that transmitted the excitation light to the resin. A reinforced industrial grade optical fiber cable protected the optical fiber for its connection to the sensor head in the extruder and its connection to the detector. The sensor and micrometer assembly are shown in *Fig. 4*. At the sensing head, the optical fiber is assembled in a sheath with a collar that holds a focusing lens. The sheath is inserted into the standard bolt sleeve and at the same time it is connected to a micrometer that can move the sheath/lens/fiber assembly in the axial direction of the sensor bolt. In this way the position of focus is moved in the radial direction of the barrel and screw while carrying out the temperature profile measurement. The resulting fluorescence transmits back through the lens to six 200-μm collection fibers that conduct the light to the photomultiplier detectors. The collection fibers act as a pinhole and the point-to-pinhole confocal design is thus achieved. The maximum length of travel for the micrometer is 3.175 mm. The spatial resolution of the sensor is 0.5 mm. For measurements taken at distances separated by less than 0.5 mm, the results will be convoluted. Although deconvolution of such data is possible using the spatial sensitivity curve developed in Ref. 14, we have not considered it necessary for these data because the spatial increments that we use are close to 0.5 mm.

The fluorescence temperature method has been described previously (12–14). This technique involves measuring the fluorescence intensity at two wavelengths and calculating the temperature from a calibration function involving the ratio of the two intensities and the applied pressure. For perylene doped into polycarbonate resin, the dye is excited at 407 nm and fluorescence is created over the range of 420 nm to 520 nm. Within this spectrum, the two wavelengths of interest are 464 nm and 475 nm, and the calibration function for the temperature measurements is:

$$T = 807.3 \frac{I_{464}}{I_{475}} - 373 + 0.57P \quad (1)$$

Fig. 4. The confocal optical sensor with micrometer movement. [Color figure can be viewed in the online issue, which is available at www.interscience.wiley.com.]

where T is the temperature in degrees Celsius, I is the intensity, and P is the pressure in MPa. *Equation 1* was obtained using a temperature-pressure calibration cell that was constructed with a standard half-inch threaded port to accommodate the sensor. Temperature measurements were made using a type J thermocouple. For the on-line measurements, pressure at the optical sensor was obtained by interpolation of pressure readings from neighboring sensors upstream and downstream in the barrel wall. Maximum pressure observed during these experiments was 27 MPa. The standard uncertainty in the temperature measurements is 1.3°C; for pressure, it is 0.03 MPa; and for the profile depth, it is 0.0125 mm, which is much less than the spatial increments used in these experiments.

As with any new measurement technique, the validity and accuracy of the measurement were examined. In our previous work, we discussed these issues, but it is appropriate to present more detail about the temperature and spatial sensitivity of the profiling sensor. From *Eq 1* we have

$$\frac{dT}{d(I_1/I_2)} = 807.3 \tag{2}$$

The measured standard uncertainty in the ratio I_1/I_2 is 0.15%, i.e.,

$$0.0015\ (I_1/I_2) = d(I_1/I_2) \tag{3}$$

Combining *Eqs 2* and *3*,

$$dT = 0.0015 \cdot 807.3\ (I_1/I_2) \tag{4}$$

Since the intensities I_1 and I_2 are approximately equal, $(I_1/I_2) = 1$, yielding an uncertainty $dT = 1.3$°C. Uncertainty in the pressure measurement accounts for an additional 0.02°C. Whereas 1.3°C is the standard uncertainty SD for a single temperature measurement, for the experiments described below, we will obtain a large number of measurements n in the steady state for which we can apply Gaussian statistics and calculate a standard error of the mean, $SD/\sqrt{n}$.

In order to maintain the uncertainty of a single temperature measurement at 1.3°C, total photon counts for each measurement needed to be greater than 10^5 counts. We have reason to be concerned about the photon count because, in carrying out temperature profile measurements, we focus the excitation light to different depths within the resin. Fluorescence from the surface yields a high count rate, but for the excitation beam focused below the surface the fluorescence production decreases because of light absorption and resorption phenomena, i.e., as excitation light traverses through the dye doped resin, it is absorbed during transit to the point of focus and the generated fluorescence is absorbed while transmitting back to the collection fibers. The phenomena are demonstrated in *Fig. 5* where we have plotted fluorescence intensity at 464 nm versus distance from the window of the sensor. In order to accommodate low intensity at large distances, we increased the count integration time whenever necessary

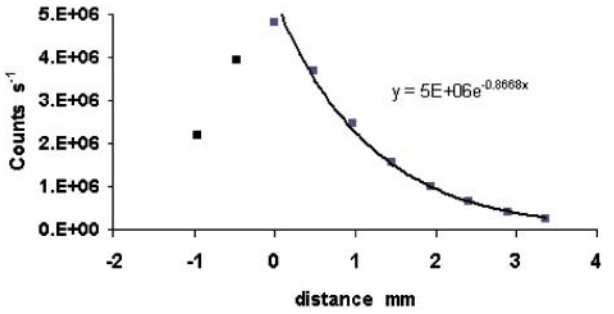

Fig. 5. Fluorescence intensity at 464 nm versus distance. [Color figure can be viewed in the online issue, which is available at www.interscience.wiley.com.]

so that total photon counts remained above 10^5. Integration times from 0.5 s to 2 s were used. Because of this need to maintain the photon count above 10^5, the technique is not sensitive enough to provide measurements in the angular direction of the screw for this application. Thus, a two-dimensional temperature space of the extruder channel at a given axial location is currently not possible.

Measuring temperature profiles requires that an accurate zero point (d = 0) on the distance scale be established; i.e., we must synchronize the micrometer reading with a determination that the focus is at the sensor sapphire window/resin interface. A search for d = 0 is carried out by measuring fluorescence intensity as a function of focus position as shown in *Fig. 5*. The maximum in this plot occurs at d = 0 because for $d < 0$ the focus is inside the window where there is no fluorescent dye and for $d > 0$ the focused light must travel through a dye absorbing medium resulting in fluorescence intensity that decreases exponentially according to Beer's law. To fix d = 0, we fit the intensity versus distance curve with an exponential function, maximizing the fit by adjusting the d = 0 position as shown in *Fig. 5*.

We note that the distances plotted in *Fig. 5* have been corrected for Snell's law effect on the light ray path. Snell's law requires that the path of the converging rays from the lens is redirected at the air/sapphire and sapphire/resin interfaces. In the small angle limit, Snell's law dictates that a change of the micrometer position Δm translates to a change in focus position in the polycarbonate Δd as $\Delta m = n_{pc}\Delta d$. where n_{pc} is the index of refraction of polycarbonate. At T = 270°C, $n_{pc} = 1.514$. Snell's law has the effect of amplifying the micrometer distance changes.

To measure temperature profiles, the micrometer was changed in steps of 0.32 mm or 0.64 mm, holding constant at each position while the fluorescence temperature was measured for approximately 10 min. A moderately long measuring time was used in order to investigate the stability of the steady state and to collect enough data to determine the uncertainty in the measurement.

Validation experiments were carried out using the 19-mm-diameter single-screw extruder instrumented with the IR temperature, fluorescence, thermocouple,

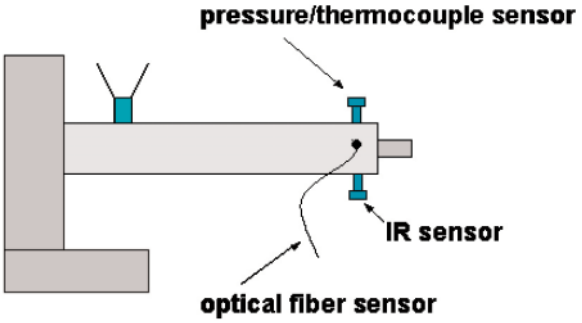

Fig. 6. The setup on the 19-mm-diameter extruder for the validation experiments is shown. [Color figure can be viewed in the online issue, which is available at www.interscience.wiley.com.]

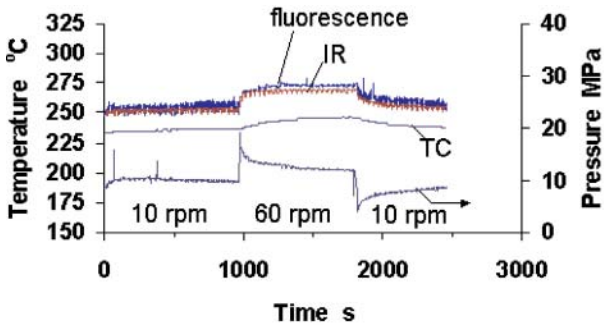

Fig. 7. Fluorescence, IR and thermocouple temperatures and pressure are plotted versus time for PC extruded with setup shown in Fig. 6. [Color figure can be viewed in the online issue, which is available at www.interscience.wiley.com.]

and pressure sensors. The setup for the validation measurements is shown in *Fig. 6*. Each sensor is located at the same axial position near the extruder exit in the transfer line, but at different angular positions so that each is monitoring a slightly different portion of the extrudate, but this difference is minimized by making measurements under steady-state flow conditions. The excitation light from the fluorescence sensor was defocused in order that it monitored an average resin temperature comparable to that obtained from the passive unfocused IR sensor. With melt zones on the extruder set at 250°C, the 6-MFR polycarbonate resin was extruded in the following sequence: 10 rpm, stepping to 60 rpm, and reducing quickly to 10 rpm. The results from all four sensors are shown in *Fig. 7*. The IR temperature and the fluorescence temperature track changes in coincidence and differ by less than 3°C over the course of the experiment. Differences can be attributed to the different locations of the two sensors and to the fact that the two sensors measure different spatial averages of temperature. Both the IR and fluorescence sensors measure resin temperature whereas the thermocouple measures the temperature of the barrel at its location. The large difference between thermocouple temperature and the temperatures measured by IR and fluorescence reinforces a well-known fact of polymer processing that thermocouples inserted in a barrel instrument port measure barrel temperature and not resin temperature (12). The results of another validation experiment can be found in figure 5 of Ref. 14.

RESULTS AND DISCUSSION

Steady-state conditions for the 63.5-mm-diameter extruder were examined by setting the focus of the excitation light to a position near the sapphire window, d = 0, where the point of focus would not be intersected by the screw flight. The 6 MFR resin was extruded using the conventional screw turning at 20 rpm with barrel temperatures set at 275°C. Steady-state temperature versus time is shown in *Fig. 8*. In this case, 290 temperature measurements yielded an average of 277.3°C with a standard uncertainty of 0.89°C and a standard error of the mean of only 0.052°C. This observation is typical of the amount of time and the number of data points that were obtained for the temperature scans described below. The largest standard error of the mean for data points in *Figs. 10*, *13* and *14* is 0.2°C.

Monitoring the dynamics of screw rotation was carried out using the conventional screw with the 6-MFR resin. The extruder was operated at a screw speed of 2.094 rad/s (20 rpm) and data were collected from the optical sensor at an acquisition frequency of once every 0.5 s, i.e., 2 Hz or six temperature measurements per screw rotation. For the data of *Fig. 9*, the excitation light was focused at a position 0.95 mm from the barrel wall. The periodic spikes in both the count data and the temperature data coincide with the periodic translation of a screw flight in front of the sensor window. The decrease in counts and increase in temperature was seen at every sixth datum point. (It is apparent that

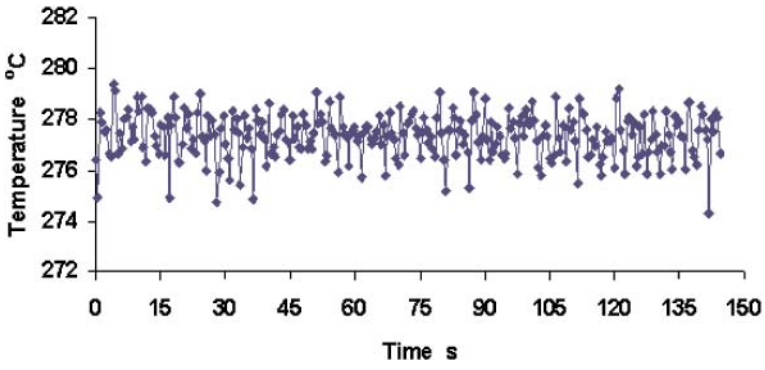

Fig. 8. Steady state fluorescence temperature measurements are plotted versus time for d = 0 and the 63.5-mm-diameter extruder at 20 rpm using 6-MFR PC resin. [Color figure can be viewed in the online issue, which is available at www.interscience.wiley.com.]

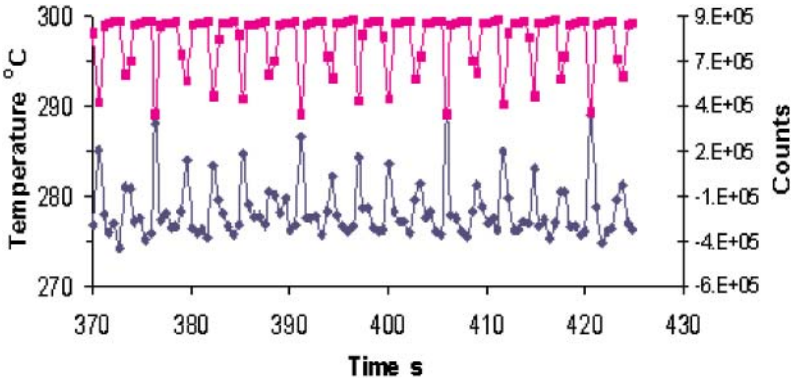

Fig. 9. Temperature (◆) and fluorescence intensity (■) versus time for d = 0.95 mm. Data are for the 63.5-mm-diameter conventional screw and the 6-MFR PC resin at a screw speed of 2.094 rad/s (20 rpm). [Color figure can be viewed in the online issue, which is available at www.interscience.wiley.com.]

the data-acquisition rate and the screw rotation were not exactly synchronized, but the discrepancy is small.) Each time a screw flight passed the window, the counts decreased as the flight cut off a part of the focused beam, but at the same time, the flight pushed a film of highly stressed resin between it and the wall. Spikes in the temperature data of 5°C to 15°C above the bulk material temperature are associated with shear heating of the thin film of molten resin between the flight and barrel wall. This heating effect between the flight tip and the barrel wall was expected, and is within the magnitude of the temperature increase expected from extrusion theory (21). The temperature of the resin in the flights was not the main focus of this study, and thus these high temperatures needed to be removed from the data set.

In order to calculate average temperatures for the position of focus, a filtering method was used to remove these high values, and only filtered data will be presented in the next sections. The discharge temperature from the extruder was measured at 287°C using a hand-held thermocouple. This measurement is not subject to the heat transfer problems associated with normal process temperature measurements owing to its isolation from heated metal parts. As will be shown later, this measurement was consistent with that measured by the optical sensor.

The temperature of the channel as a function of the channel depth was measured by moving the focus point away from the barrel wall. Temperature profiles are shown by *Fig. 10*. At a screw speed of 2.094 rad/s (20 rpm), the temperature was 278°C at a distance of 0.95 mm from the barrel wall. The temperature was the lowest in the center of the channel and increased at the barrel wall and at the root of the screw. The temperature gradient at the screw root indicated that an energy flux in through the screw was occurring. This energy flux in was caused by the temperature of the screw being higher than that of the PC resin near the root. The screw had a higher temperature at this axial location due to the energy conducting from the hotter screw tip down the metal screw. For this case, the bulk temperature of the extrudate was measured using a hand-held thermocouple at 287°C. The temperature of the screw tip would be expected to approach the temperature of the discharge, and the high thermal conductivity of the metal screw will conduct energy back to the P19 position and provide a high surface temperature at the screw root. The PC resin temperature near the barrel was about 279°C, a temperature just slightly higher than the barrel temperature of 275°C, indicating essentially zero energy transport through the barrel wall.

As previously discussed, the bulk temperature of the extrudate measured for this case using a hand-held thermocouple was 287°C. Calculation of the bulk temperature based on the data in *Fig. 10* would require knowledge of the velocity fields, which are not known (6, 7). However, spatially averaged temperatures T_{avg} can be calculated according to

$$T_{avg} = \frac{\int_0^d T \cdot T(x)dx}{\int_0^d T(x)dx} \quad (5)$$

where d is the depth of the profile and $T(x)$ is a functional expression of the temperature profile. To employ *Eq 5*, the measured profiles were fit with a polynomial

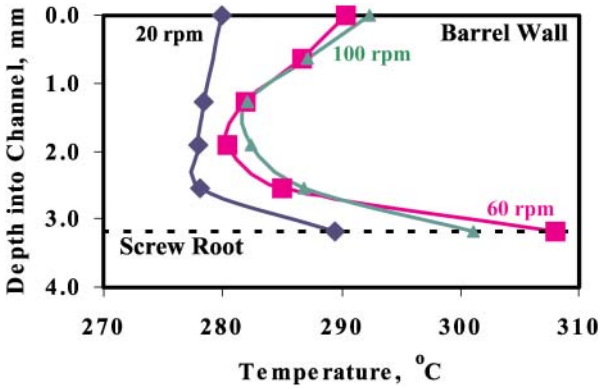

Fig. 10. Temperature profiles in the 63.5-mm-diameter conventional screw for screw speeds of 2.094 rad/s (20 rpm), 6.28 rad/s (60 rpm) and 10.47 rad/s (100 rpm) and the 6-MFR PC resin. [Color figure can be viewed in the online issue, which is available at www.interscience.wiley.com.]

Table 1. Measured Temperatures for 63.5-mm-Diameter Conventional Screw. T_{avg} Is at an Axial Position of 19 Diameters From the Start of the Screw While T_{TC} Is at the Discharge.

rpm	MFR	Rate, kg/h	T_{avg}	T_{TC}
20 (2.094 rad/s)	6	26	279°C	287°C
60 (6.28 rad/s)	6	75	283°C	311°C
100 (10.47 rad/s)	6	89	284.8°C	324°C
60 (6.28 rad/s)	23	78	274°C	288°C

expression and integrated. We note that T_{avg} is not equivalent to the bulk resin temperature, but is a process average describing the steady state at the axial position of the sensor. In the ensuing discussion we will compare T_{avg} with the hand-held thermocouple measurement, T_{TC}. For the 20-rpm profile of *Fig. 10*, T_{avg} is 279°C, a temperature that is consistent with the downstream measured T_{TC} = 287°C; i.e., as the material moves downstream viscous energy dissipation in the screw channels and conical tip assembly increases the bulk temperature of the resin.

The effect of screw speed on the temperature profile is shown in *Fig. 10* where these data are for the 6-MFR PC resin and the conventional screw. As expected, the channel temperatures increased with increasing screw speed. Spatially averaged fluorescence temperatures, T_{avg}, are 279°C at 2.094 rad/s (20 rpm), 283°C at 6.28 rad/s (60 rpm) and 284.8°C at 10.47 rad/s (100 rpm), and the extrudate temperatures measured by hand-held thermocouple, T_{TC}, were 287°C, 311°C, and 324°C at screw speeds of 2.094 rad/s (20 rpm), 6.28 rad/s (60 rpm), and 10.47 rad/s (100 rpm), respectively (see *Table 1*). The large difference in the thermocouple temperature between 6.28 rad/s (60 rpm) and 10.47 rad/s (100 rpm), 13°C, was not reflected in T_{avg} for which the difference was only 1.8°C. This is because the fluorescence temperatures obtained at 10.47 rad/s (100 rpm) have been compromised by solids or cooler material in the flow and in view of the sensor. The effect is shown in *Fig. 11*, where we have plotted temperature versus time for a screw speed of 10.47 rad/s (100 rpm) and d = 1.27 mm. Temperature varies over a wide range, from 250°C to 295°C. The very low temperatures observed here are evidence for solids or cooler material in the flow; i.e., pellets that have not reached the processing temperature at this axial location, position P19, in the extruder. A conventional screw turning at high rpm conveys resin pellets through the extruder at such a rapid rate that some of the pellets do not fully blend (or devitrify) into the melt stream at position P19 on this extruder (25). If the maximum temperatures at each position are used to calculate T_{avg} for a speed of 10.47 rad/s (100 rpm), we obtain a value T_{avg} = 296°C or exactly 13°C above the spatial average for 6.28 rad/s (60 rpm), the same difference as observed with the hand-held thermocouple. This result indicates that the resin pellets are entirely blended at the exit of the extruder where the hand-held thermocouple measurements were made.

The dynamics of change from one process condition to another can be seen in *Figs. 11* and *12*, where the temperature dynamics associated with changes from a speed of 10.47 rad/s (100 rpm) to 2.094 rad/s (20 rpm) and from 2.094 rad/s (20 rpm) to 6.28 rad/s (60 rpm) for the 6 MFR PC resin are plotted. In *Fig. 11*, the wide temperature swings associated with solids in the flow disappear after the change to 2.094 rad/s (20 rpm) and a much smaller temperature spread was observed as the average temperature of the resin decayed slowly over time. No data were collected as speed was decreased to 2.094 rad/s (20 rpm) resulting in the 30 s gap in the data.

The temperature profiles at the higher screw speeds were similar to that at a screw speed of 2.094 rad/s (20 rpm), as shown by *Fig. 10*. The temperature was the

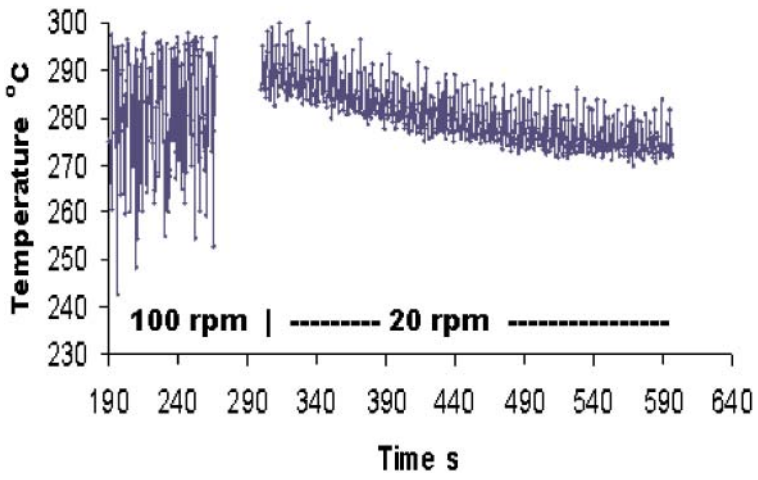

Fig. 11. The transition from A (10.5 rad/s (100 rpm) to B (2.094 rad/s (20 rpm) screw speed is reflected in the change in temperature for the 63.5-mm-diameter conventional screw and the 6-MFR PC resin. Depth of focus was 1.27 mm. [Color figure can be viewed in the online issue, which is available at www.interscience.wiley.com.]

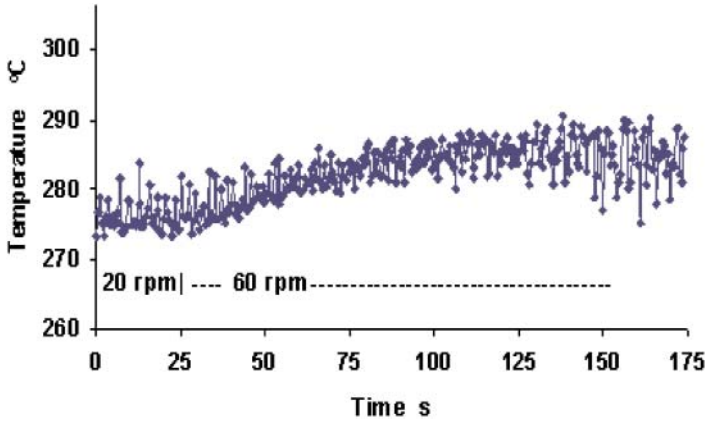

Fig. 12. Temperature versus time for change from 2.094 rad/s (20 rpm) to 6.28 rad/s (60 rpm) for the 63.5-mm-diameter conventional screw and the 6-MFR PC resin. [Color figure can be viewed in the online issue, which is available at www.interscience.wiley.com.]

lowest in the center of the channel, and the temperatures increased near the root of the screw and near the barrel wall. As expected the temperature of the resin near the screw root increased with increasing screw speed, consistent with the extrudate temperatures. The temperatures near the barrel wall at speeds of 60 and 100 rpm, however, are more difficult to explain. These temperature profiles indicate an energy flux from the barrel wall into the center of the channel; i.e., the barrel is in a heating mode. The barrel temperature, however, was maintained at 275°C, a temperature less than the measured resin temperature near the wall of 287°C, suggesting that the barrel is in a cooling mode. The reason for this discrepancy is unknown, but it may be related to the higher resin temperatures contributed from resin flow across the flight tip where energy dissipation is relatively high.

The effect of resin viscosity on the temperature profile at a screw speed of 6.28 rad/s (60 rpm) using the conventional screw is shown by *Fig. 13*. The lower viscosity of the 23 MFR PC resin reduced the level of viscous dissipation in the screw channels, and this is indicated by its temperature profile and T_{avg} of 274°C, both considerably lower than that for the 6-MFR resin. These data are consistent with measured extrudate temperatures of 288°C and 311°C for the 23-MFR and 6-MFR resins, respectively, and are consistent with extrusion theory (21).

The temperature profile for the mixing screw was measured using the 6-MFR PC resin at screw speeds of 2.094 rad/s (20 rpm) and 6.28 rad/s (60 rpm) and the temperature profiles are shown in *Fig. 14*. Like the conventional screw, the mixing screw had temperature gradients near the screw that indicated an energy flux in through the screw root, but at the barrel wall an energy flux out is indicated. A striking feature of the temperature profiles is that the temperature gradient for both screw speeds approaches zero at a channel depth of approximately 1.5 mm. This location is near the position of the undercut of the mixing flight of the mixing section, 1.40 mm. These data suggest that the cold material was entering this mixing clearance and reducing the temperature gradient in the region, especially in the shallower channel on the right-hand side of *Fig. 3*. This channel on the right-hand side is decreasing in the depth with the downstream flow direction, trapping and mixing colder material into the surrounding hot resin (20). As the sensor probes deeper into the material

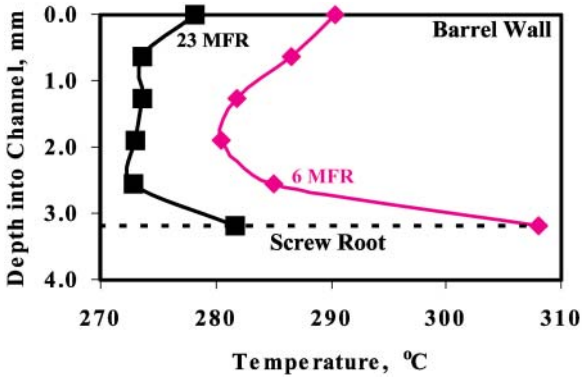

Fig. 13. Temperature profile for 63.5-mm-diameter conventional screw at 6.28 rad/s (60 rpm) using 6-MFR and 23-MFR PC resins. [Color figure can be viewed in the online issue, which is available at www.interscience.wiley.com.]

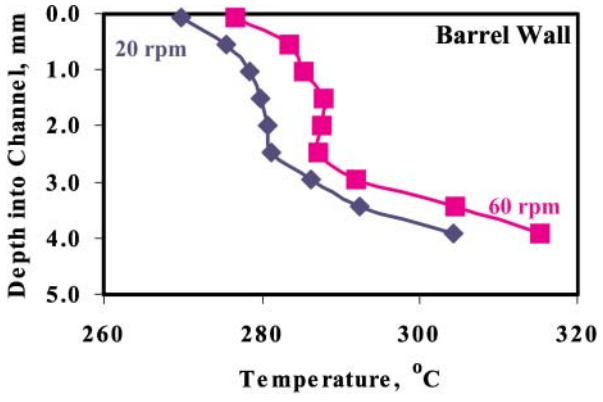

Fig. 14. Temperature profiles for 63.5-mm-diameter mixing screw using 6-MFR resin at 2.094 rad/s (20 rpm), and 6.28 rad/s (60 rpm). [Color figure can be viewed in the online issue, which is available at www.interscience.wiley.com.]

toward the screw root, a sharp increase in the gradient appeared like that for the conventional screw due to energy conduction from the screw root.

As shown by *Fig. 14*, the temperature measurements for the mixing screw were performed at channel depths from 0 (barrel wall) to about 3.8 mm. At a depth of 3.8 mm, the sensor was measuring temperatures away from the screw root in the majority of the screw rotation. At the pushing side of the shallow channel, however, the channel depth decreased to 3.6 mm, as shown by *Fig. 3*. When the sensor was near this shallow region the light path was obstructed and caused the flight width to appear wider than actual. As previously discussed, these events where the light path was obstructed by the flight were filtered from the data set.

The temperature profiles shown by *Fig. 14* are temperatures that have been averaged over the 360° rotation of the flight (with the flight regions removed via filtering). As discussed previously, this averaging prevented temperature measurements in the angular direction. For temperature measurements for the conventional screw, this averaging did not create a significant complication to the measurement because of the relatively high aspect ratio of the width of the channel to the channel depth, i.e., the ratio was about 58 based on the channel width in the angular direction. The mixing screw, however, has a complicated geometry with temperature gradients that are predicted to be complex (22). Although this is the first time that the temperature was measured in the channels of a mixing screw, the results are confounded by the variable geometry in the path of the sensor. These data, however, do provide a basis for further numerical simulations for the screw utilizing rate, boundary conditions, and material properties that are specific to this process.

Like the conventional screw, the T_{avg} values were calculated using *Eq 5*. T_{avg} for screw speeds of 2.094 rad/s (20 rpm) and 6.28 rad/s (60 rpm) were 283°C and 290°C respectively, and the respective hand-held thermocouple measurements were 287°C and 309°C (see *Table 2*). One should expect slightly higher temperatures for the extrudate from the mixing screw given the additional shearing that occurs at the undercut flights of this screw.

To our knowledge, this is the first time that temperatures were measured in a rotating screw channel as a function of channel depth using a non-invasive technique. As such, comparisons to previously measured data are not possible. Comparison of the experimental results with numerically simulated data is also not possible because of the complicated set of boundary conditions, complex geometries, and resin properties. These data, however, do provide a unique set of conditions for future simulations, and they are consistent with extrusion theory.

These observations are in concurrence with results of earlier studies by McCullough and Spalding (6) and recent studies by Brown *et al.* (2, 3), who used a thermocouple mesh at the end of a single-screw extruder to measure temperature profiles. Brown *et al.* used both a conventional metering screw and a mixing screw in an extruder similar to ours, 63.5-mm-diameter screw with L/D of 24. Their measurements, for polyethylene, showed considerable viscous dissipation when processed at 200°C. For the conventional screw at low rpm, temperature profiles had small gradients, and at high rpm they also observed thermal instabilities associated with solids conveying. In all of these studies, energy flux in from the core of the screw is prominent feature of the process. Our observations, taken together with those using thermocouple meshes, provide a detailed picture of thermal patterns, dynamics and instabilities of single-screw extrusion.

CONCLUSIONS

The fluorescence analytical technique was used to measure the temperature profiles in a rotating screw channel of a single-screw extruder. Because the fluorescent dye is soluble in the resin, the temperature deduced from its spectra reflect the resin temperature in the dye's molecular neighborhood. The data collected provided a unique view of the temperature profiles that are unobtainable using other methods such as thermocouple probes and IR techniques.

Temperature profiles for the metering section of a conventional screw as a function of distance away from the barrel surface; i.e., into the channel of the screw, clearly showed that an energy flux in through both the barrel wall and the root of screw was occurring. Temperature data that were measured as a function of screw speed and resin MFR were consistent with extrusion theory in that temperatures are expected to increase with decreasing MFR and increasing screw speed and to be higher at the boundaries where the shear stress is highest (21).

The method provided a very unique view of the temperatures in a high-performance mixing screw. These data show a region at 1.5 mm from the barrel wall where the temperature gradient approaches zero, which is consistent with the movement of cool resin from the conveying sector, over the undercut and into the shearing/melting sector of the screw. The large temperature gradient near the root of the screw is indicative of high shear that yields improved mixing and melting in this screw design.

Table 2. Measured Temperatures for 63.5-mm-Diameter Mixing Screw. T_{avg} Is at an Axial Position of 19 Diameters From the Start of the Screw While T_{TC} Is at the Discharge.

rpm	MFR	Rate, kg/h	T_{avg}	T_{TC}
20 (2.094 rad/s)	6	33	283°C	287°C
60 (6.28 rad/s)	6	87	290°C	309°C

REFERENCES

1. M. A. Spalding, K. S. Hyun, and J. Vlachopoulos, *The SPE Guide on Extrusion Technology and Troubleshooting,* Chap. 6, J. Vlachopoulos and J. Wagner, eds., Society of Plastics Engineers, Brookfield, Conn. (2001).
2. E. C. Brown, A. L. Kelly, and P. D. Coates, *SPE ANTEC Tech. Papers*, **49**, 77 (2003).
3. A. L. Kelly, E. C. Brown, and P. D. Coates, *SPE ANTEC Tech. Papers*, **49**, 82 (2003).
4. H. Kim and E. Collins, *Polym. Eng. Sci.*, **11**, 83 (1971).
5. T. W. McCullough and B. Hilton, *SPE ANTEC Tech. Papers*, **38**, 927 (1992).
6. T. W. McCullough and M. A. Spalding, *J. Reinforced Plastics and Composites*, **16**, 1622 (1997).
7. J. vanLeeuwen, *Polym. Eng. Sci.*, **7**, 98 (1967).
8. H. Kim and E. Collins, *Polym. Eng. Sci.*, **11**, 83 (1971).
9. M. Esseghir and V. Sernas, *Adv. Polym. Technol.*, **13**, 133 (1994).
10. E. Haberstroh, L. Jakisch, E. Henssge, and P. Schwarz, *Macromolecular Materials and Engineering*, **287**, 203 (2002).
11. C. Maier, *Polym. Eng. Sci.*, **36**, 1502 (1996).
12. A. J. Bur, M. G. Vangel, and S. C. Roth, *Polym. Eng. Sci.*, **41**, 1380 (2001).
13. A. J. Bur, M. G. Vangel, and S. Roth, *Applied Spectroscopy*, **56**, 174 (2002).
14. K. B. Migler and A. J. Bur, *Polym. Eng. Sci.*, **38**, 213 (1998).
15. Identification of a commercial product is made only to facilitate experimental reproducibility and to describe adequately the experimental procedure. In no case does it imply endorsement by NIST nor does it imply that it is necessarily the best product for the experiment.
16. T. A. Hogan, M. A. Spalding, K. S. Cho, and C. I. Chung, *SPE ANTEC Tech. Papers*, **48**, 384 (2002).
17. M. A. Spalding, J. Dooley, K. S. Hyun, and S. R. Strand, *SPE ANTEC Tech. Papers*, **39**, 1533 (1993).
18. C. I. Chung and R. A. Barr, U.S. Patent 4,405,239 (1983).
19. J. A. Myers and R. A. Barr, *SPE ANTEC Tech. Papers*, **48**, 154 (2002).
20. S. A. Somers, M. A. Spalding, J. Dooley, and K. S. Hyun, *SPE ANTEC Tech. Papers*, **48**, 307 (2002).
21. Z. Tadmor and I. Klein, in *Engineering Principles of Plasticating Extrusion*, Van Nostrand Reinhold Co., New York (1970).
22. M. A. Spalding and K. S. Hyun, *SPE ANTEC Tech. Papers*, **49**, 229 (2003).